

Existence of dual topological phases in Sn -based ternary chalcogenides

Ramesh Kumar and Mukhtiyar Singh*

*Computational Quantum Material Design (CQMD) Lab, Department of Applied Physics,
Delhi Technological University, New Delhi-110042, India*

arXiv:2411.06088v2 [cond-mat.mtrl-sci] 19 Nov 2024

Abstract

It is quite intriguing to investigate the transition from a topological insulator (TI) phase to topological crystalline insulator (TCI) phase in a material as the latter has an advantage over the former in controlled device applications. This work investigates the existence of this dual topological behavior in Sn -based ternary chalcogenides family $PbSnX_2$ ($X=S, Se, Te$) under the hydrostatic pressure using first-principles approach. These materials are dynamically stable at ambient and elevated pressure conditions up to which the topological phase transitions (TPTs) are studied. This family have a topologically trivial ground state with direct band gap values 0.338 eV, 0.183 eV and 0.217 eV for $PbSnS_2$, $PbSnSe_2$ and $PbSnTe_2$, respectively. The first TPT i.e., TI phase for these materials is observed, under the effect of external pressure of 5 GPa, 2.5 GPa and 3.5 GPa, with a single band inversion at F -point in the bulk band structure and an odd number of Dirac cones along the (111) surface. A further increase in pressure to 5.5 GPa, 3 GPa and 4 GPa results in another band inversion at Γ -point and an even number of Dirac cones along the (111) plane. These even number of band inversions suggest that $(\bar{1}2\bar{1})$ surface has mirror symmetry around $(\bar{1}0\bar{1})$ plane and hence, the TCI phase is obtained. This TCI phase is further corroborated with even value of mirror Chern number calculated using winding of Wannier charge centers.

Keywords: Topological phase transition, ternary chalcogenides, first-principles calculations, topological crystalline insulators, mirror Chern number.

I. INTRODUCTION

A new phase of matter with unusual metallic edge/surface states known as topological materials (TM) has been studied intensively in recent years [1–6]. The TMs can be divided into few categories such as topological insulators (TIs) [3–6], topological crystalline insulators (TCIs) [7–9], Dirac semimetals (DSMs) [10, 11], Weyl semimetals (WSMs) [12, 13], nodal line semimetals (NLSMs) [14, 15], Z_2 topological semimetals [16, 17] and triply degenerate node semimetals [18, 19], etc. The metallic Dirac-like electronic states on the surface of the crystal with insulating bulk are the signature of the existence of TI. These metallic edge/surface states appear in the presence of spin-orbit coupling (SOC) which are protected

* mukhtiyarsingh@dtu.ac.in; msphysik09@gmail.com

by time-reversal symmetry (TRS) and provides robust spin-polarized conduction channels [1–6]. These materials have potential applications in low-power high-speed electronic and spintronic devices, quantum computing, and thermoelectric applications [20–22] etc. The careful alteration in the strength of SOC plays an important role in realizing topological phases in specific materials. The hydrostatic pressure is a non-destructive way of enhancing SOC without affecting the charge neutrality of the materials. The binary and ternary materials like Bi_4Br_4 [23], LaAs [16], YbAs [24], LnSb ($\text{Ln}=\text{La, Gd, Tm}$) [17, 25], YX ($\text{X}=\text{As, Sb, Bi}$) [26, 27] and KNa_2Bi [28], BiTeI [29], Bi_2S_3 [30], BiTeBr [31] have shown the topological phase transition (TPT) with hydrostatic pressure.

The term “topological crystalline insulators,” has been introduced by L. Fu, which defines a class of materials having robust topological states and are protected by crystalline symmetries [7]. This new phase was first proposed in SnTe and later angle-resolved photoemission spectroscopy (ARPES) verified the topological surface states (TSSs) in the (001) plane of this material [8]. Unlike TIs, TCIs have persisted protection by mirror symmetry even when TRS is broken. It is quite intriguing to investigate the TPT from TI to TCI in a material. TCI phase is more robust against impurities or defects and has diverse and tunable topological characteristic states [7, 32]. TCI materials hold higher-order topological hinge or corner states which can be identified with different topological invariants depending on the crystal symmetries [33, 34] and can have potential applications in stable qubits and novel electronic devices [7, 32–34]. The TCI phase has an advantage over the TI phase for controlled device applications such as a topological field effect transistor [32].

The narrow band-gap semiconductors are amongst the highly sought-after materials to realize TPT. Several narrow gap IV-VI semiconducting materials such as PbTe , SnSe , SnS , TlSe , TlS , and $\text{Pb}_{1-x}\text{Sn}_x\text{X}$ ($\text{X} = \text{Se, Te}$) have been studied for the existence of TIs and TCIs phases [35–39]. Other than these, the ternary chalcogenides TlXY_2 ($\text{X} = \text{Sb, Bi}$; $\text{Y} = \text{Te, Se}$) have also been reported as strong TIs [40, 41] but the TCI phase has not been explored in these materials except for TlBiS_2 and TlSbS_2 [42]. The present study focuses on the realization of TI and TCI phases in ternary chalcogenides PbSnX_2 ($\text{X} = \text{S, Se, Te}$) with the application of external hydrostatic pressure. For this family, trivial to non-trivial phase are obtained with single band inversion at Γ -point under hydrostatic pressure. With further increases in pressure, a pair of Dirac cones are observed along the (111) plane and made these systems trivial again. However, a TCI phase emerges at this elevated pressure

as confirmed by non-trivial TSSs along $(\bar{1}2\bar{1})$ plane which is symmetric around the mirror plane $(\bar{1}0\bar{1})$.

II. COMPUTATIONAL METHODOLOGY

The structural optimization and electronic structure calculations based on the density functional theory (DFT) approach [43, 44] were performed using the projector augmented-wave (PAW) [45] method as implemented in the Vienna Ab initio Simulation Package (VASP) [46]. The PAW potentials for Pb ($6s^26p^2$) with 4 valence electrons, Sn ($5s^25p^2$) with 4 valence electrons, and S ($3s^23p^4$), Se ($4s^24p^4$), Te ($5s^25p^4$) with 6 valence electrons configuration were used for the calculations. The exchange and correlation energy were calculated with the generalized gradient approximation of Perdew–Burke–Ernzerhof (GGA-PBE) [47] and modified Becke–Johnson (mBJ) [48] functionals. The effect of SOC was included in all calculations except in ionic optimization. The total energies convergence criterion of 10^{-6} eV was adopted along with a finer $9 \times 9 \times 5$ gamma-centered k-mesh. The plane-wave cut-off energies for PbSnX_2 ($X=\text{S, Se, Te}$) were kept at 380 eV, 310 eV and 260 eV, respectively. The phonon calculations were performed using the PHONOPY code [49]. The Z_2 topological invariants were calculated using the product of parities at time reversal invariant momenta (TRIM) points as per the Kane and Mele model [6]. Wannier90 code [50] was used to obtain maximally localized Wannier functions (MLWFs) and to parametrize a tight-binding (TB) Hamiltonian. This TB Hamiltonian was used to obtain the surface density of state (SDOS) using the Green function approach as implemented in the WannierTools code [51].

III. RESULTS AND DISCUSSION

A. Crystal structure and stability analysis

The ternary chalcogenides PbSnX_2 ($X=\text{S, Se, Te}$) have adopted a rhombohedral crystal structure (space group $R\bar{3}m$ (166)) (FIG. 1 (a)) and are isostructural to the well-studied TlBiTe_2 , TlBiSe_2 , and TlBiS_2 materials [52–56] which have also been experimentally synthesized (crystal structure in suppl. information (FIG. S1)). This family has a Pb-X-Sn-X-Pb-sequence along the *three-fold axis*. The Pb/Sn layers are sandwiched between the chalcogenides layers as shown in FIG. 1 (a, b). The hexagonal supercell and the bulk Brillouin

zone (BZ) with projected surfaces along (111) and $(\bar{1}\bar{2}\bar{1})$ are shown in FIG. 1 (a, c). The surface BZ of the (111) and $(\bar{1}\bar{2}\bar{1})$ planes are represented in FIG. S2. Both Pb and Sn atoms act as an inversion center with atomic coordinates Pb (0, 0, 0), Sn (0.5, 0.5, 0.5) and X ($\pm v$, $\pm v$, $\pm v$) sites. As hydrostatic pressure is isotropic in nature which, therefore, does not alter the symmetry of the systems for the entire studied pressure range. The optimized lattice parameters for this family are given in TABLE 1.

TABLE I. Lattice parameters (in Å) of the ternary chalcogenides PbSnX_2 (X=S, Se, Te) family. Also, the bulk band energy gap at Γ - and F -points using TB-mBJ functional.

Materials	Lattice parameters	Energy gap at F -point (Bandgap, E_g)	Energy gap at Γ -point
PbSnS_2	$a = b = 4.201$; $c = 20.449$	0.338 eV	0.377 eV
PbSnSe_2	$a = b = 4.343$; $c = 21.262$	0.183 eV	0.215 eV
PbSnTe_2	$a = b = 4.589$; $c = 22.538$	0.217 eV	0.235 eV

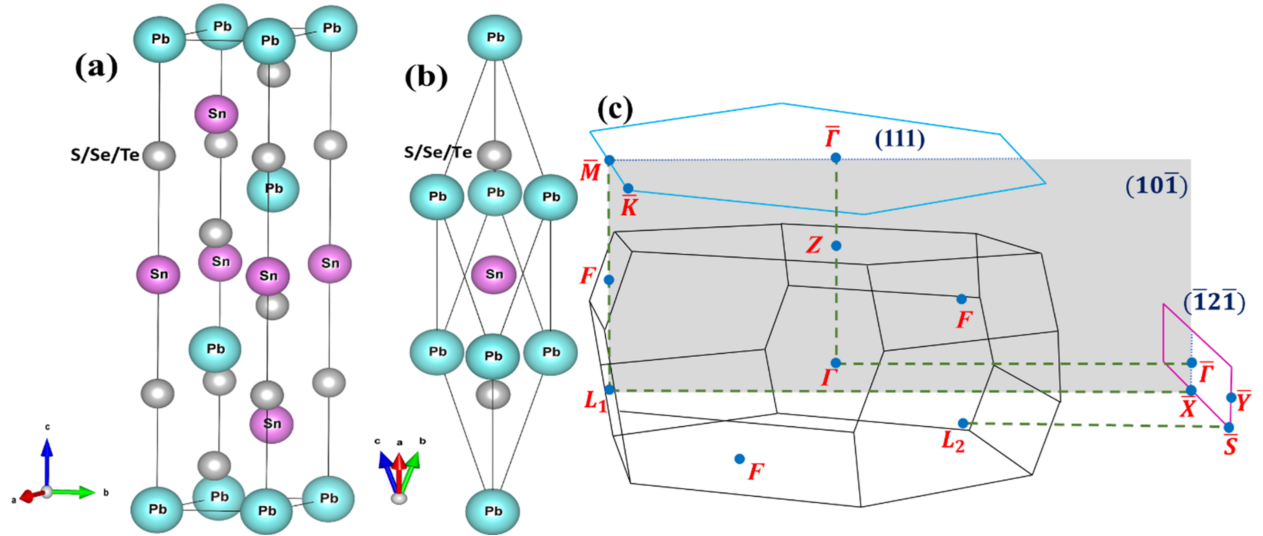


FIG. 1. The crystal structure of PbSnX_2 (X=S, Se, Te) (a) conventional hexagonal structure, (b) primitive unit cell, and (c) The bulk Brillouin zone (BZ) of primitive rhombohedral cell with projections on surface Brillouin zones.

The surface electronic structure for the TCI systems significantly depends on the orientation of the crystal face. We have considered two surfaces of the rhombohedral structure. L_1 - and F -points are projected to \bar{M} -point of the (111) plane whereas L_1 - and L_2 - points are projected on \bar{X} - and \bar{S} -points, respectively, on $\bar{1}\bar{2}\bar{1}$ plane. The $\bar{\Gamma}$ -points as the center of

both the planes are projections of the center of BZ i.e., Γ -point. The $(\bar{1}0\bar{1})$ mirror plane is perpendicular to the $(\bar{1}2\bar{1})$ surface plane and projected along the $\bar{\Gamma}-\bar{X}$ direction as shown in FIG. 1 (c). Further, we have studied the stability of PbSnX_2 ($X=\text{S, Se, Te}$) at ambient and elevated pressures via the phonon dispersion spectrum. The absence of negative frequencies at ambient and higher-pressures values as shown in FIG. S3 shows the stability of these materials. It has been noted that TPT in these materials takes place within this studied stability range of hydrostatic pressure.

B. The electronic structure at ambient pressure

It is an established fact that the prediction of ground state using DFT is highly depend upon the choice of *exchange-correlation functional* corresponding to different material systems. To choose a relevant and accurate functional for our study, we performed the *ab initio* calculation with two major functional i.e., GGA-PBE and mBJ for the experimentally synthesized TlBiS_2 material, which is isostructural to our studied systems. We found that the mBJ functional predicts the true ground state of TlBiS_2 with the band gap of 0.36 eV which is in excellent agreement with its experimental value of 0.35 eV [52–54] (see suppl. FIG. S4). Therefore, we used mBJ functional for further investigations of PbSnX_2 ($X=\text{S, Se, Te}$). However, the PBE-GGA has been quite successful in predicting the true ground state of binary chalcogenide materials [35, 37, 39, 57, 58] but in the case of this ternary chalcogenide family, it predicts an inaccurate ground state (FIG. S5). FIG. 2 (a, c, e) depicts the bulk band structure of PbSnX_2 ($X=\text{S, Se, Te}$) materials using mBJ functionals. The *p-orbital* of the Pb/Sn in the conduction band (CB) and *p-orbitals* of chalcogenide elements S/Se/Te in the valence band (VB) mainly contribute near the Fermi energy. No inverted contribution of the orbitals near the Fermi level is observed in these materials and hence they are topologically trivial semiconductors with the direct band at Γ -point. The energy gap of these materials at Γ - and F -points in bulk band structure is represented in TABLE 1. The absence of Dirac cones in SDOS along the (111) plane (FIG. 2 (b, d, f)) in these materials also establishes their topologically trivial state at ambient pressure.

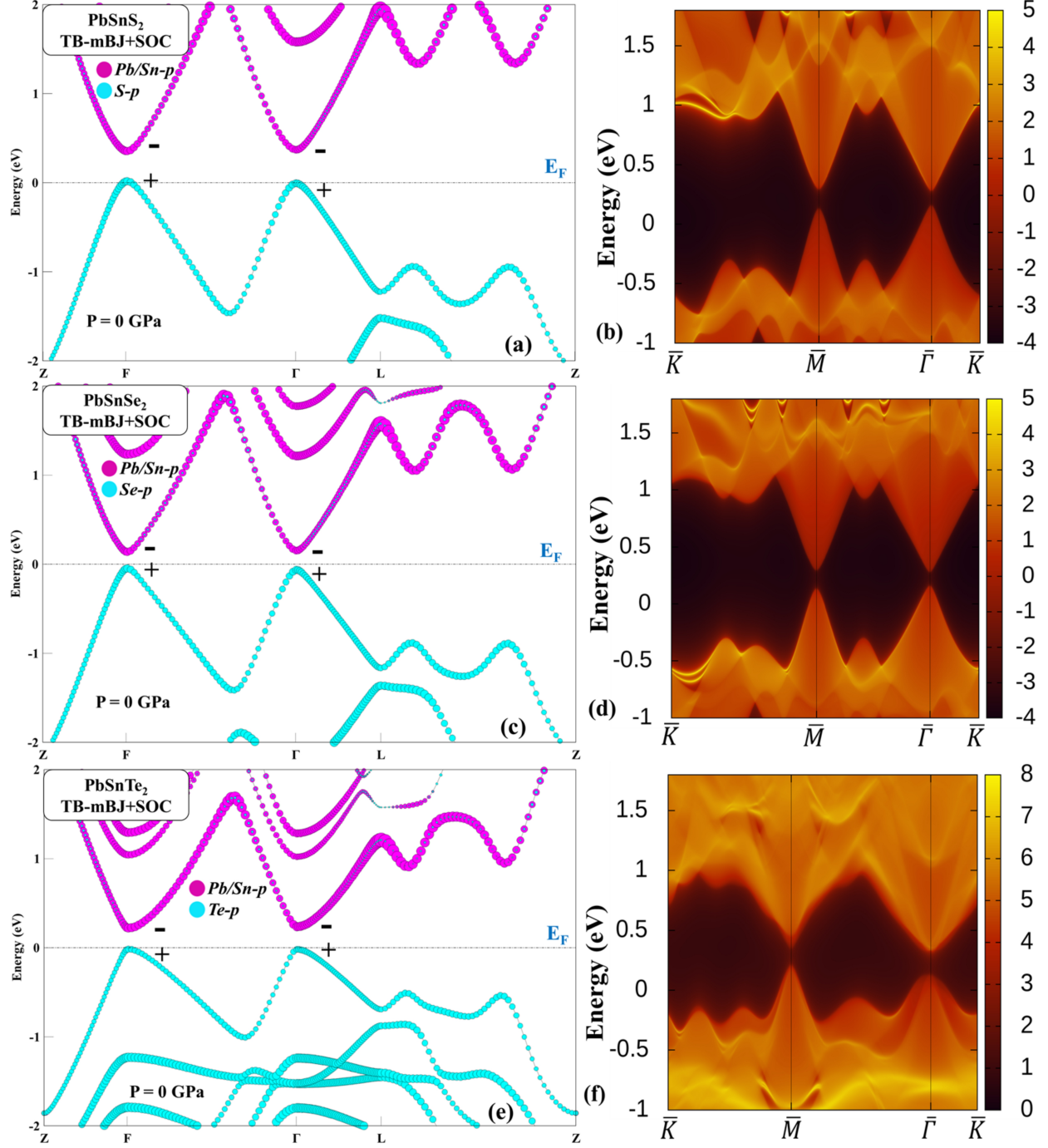


FIG. 2. (a, c, e) The bulk band structure using mBJ+SOC functional, (b, d, f) The density of states (SODS) along (111) plane of the systems PbSnX_2 ($X=\text{S, Se, Te}$) at ambient pressure.

C. The effect of hydrostatic pressure on electronic structure

In the preceding section, we have established the topologically trivial semiconducting nature of PbSnX_2 ($X=\text{S, Se, Te}$) at ambient pressure. Now, we have included the effect of hydro-

static pressure to tune the bulk electronic structure of these materials. The compressive nature of the hydrostatic pressure has performed the isotropic reduction in the lattice parameters and hence tuned the eigenstates of these systems. The application of hydrostatic pressure on PbSnX_2 ($X=\text{S, Se, Te}$) results in the TPT (FIG. 3 (a, c, e)) at 5 GPa, 2.5 GPa and 3.5 GPa, respectively. An inverted contribution of p -orbitals of chalcogenide elements S/Se/Te in CB and Pb/Sn in VB is observed at F -point, whereas no change in orbital contribution is observed at Γ -point as shown in the insets of FIG. 3 (a, c, e). The TPT pressure for PbSnTe_2 is higher than PbSnSe_2 , which is due to the higher energy gap of this material at the F -point. The SDOS along the (111) plane of these materials shows the presence of a single Dirac cone at Γ -point in surface BZ as shown in FIG. 3 (b, d, f).

A further increase in hydrostatic pressure tunes the bulk band structure at the Γ -point and band inversion at this TRIM point also takes place as shown in FIG. 4 (a, c, e). The inverted contribution of the p -orbitals of chalcogenide elements S/Se/Te in CB and Pb/Sn in VB has verified the TPT at Γ -point. Now, there is an even number of band inversions in these systems which makes them topologically weak insulators or topologically trivial systems. A pair of Dirac cones in SDOS at $\bar{\Gamma}$ -point and \bar{M} -point along the (111) plane as shown in FIG. 4 (b, d, f) also establishes the presence of an even number of band inversions in PbSnX_2 ($X=\text{S, Se, Te}$). To verify whether these materials, with even number of band inversions, are topologically weak insulators or topologically trivial, further, we have calculated Z_2 topological invariants.

D. Z_2 topological invariants

The topologically non-trivial nature of the PbSnX_2 ($X=\text{S, Se, Te}$) family under applied hydrostatic pressure can also be verified with the help of Z_2 topological invariants. These materials have TRS as well as inversion symmetry, so their Z_2 topological invariants can be calculated from the product of parities of all valance bands at TRIM points. According to Kane and Mele model [6], for a three-dimensional (3D) material, there are four Z_2 topological invariants ($\nu_0; \nu_1\nu_2\nu_3$) are required to calculate at eight TRIM points, which were defined by the following equations;

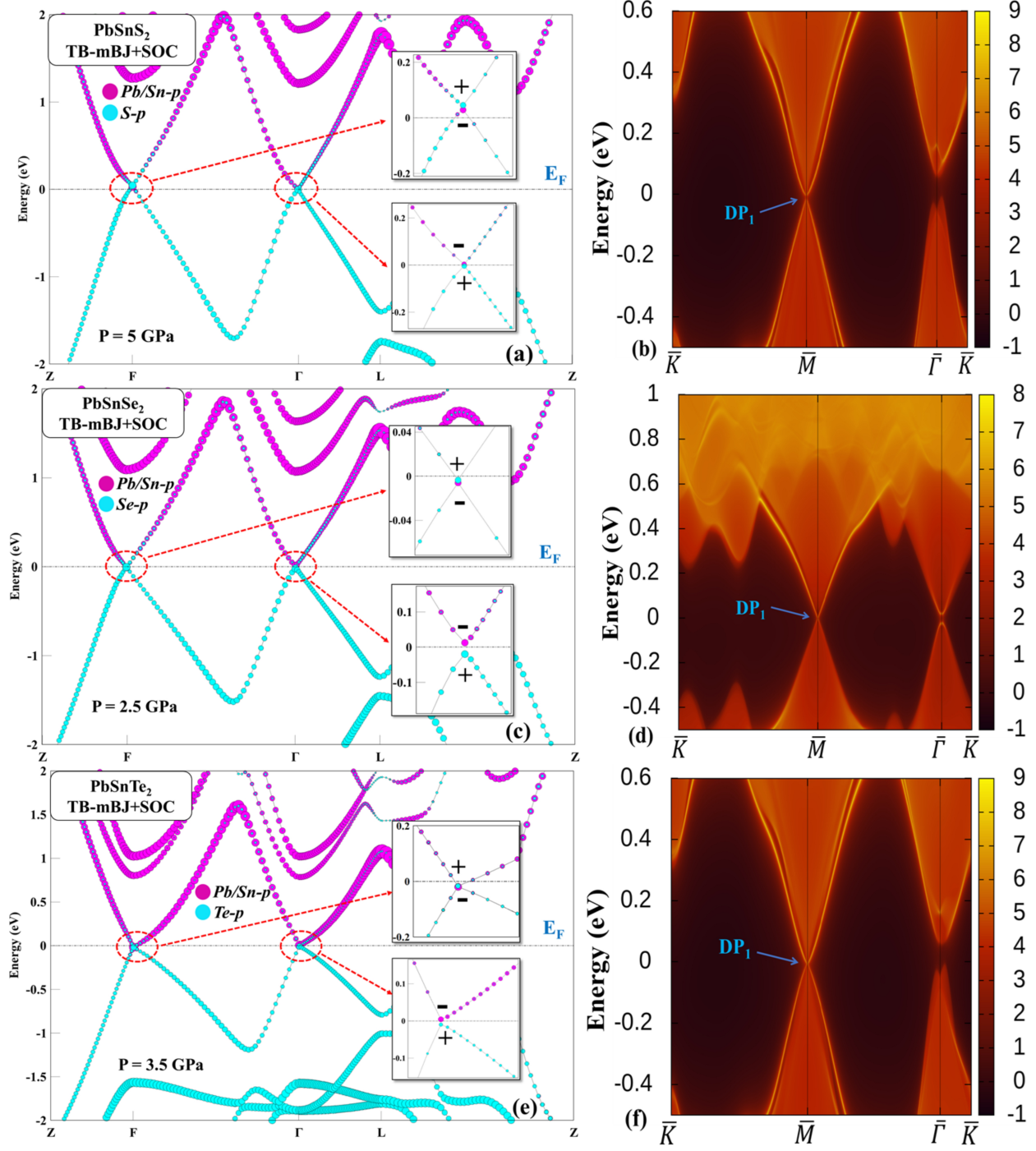


FIG. 3. (a, c, e) The bulk band structure with band inversion at F -point, (b, d, f) The surface density of states (SODS) along (111) plane of the systems PbSnX_2 ($X=\text{S, Se, Te}$) at elevated pressure with marked Dirac point (DP_1).

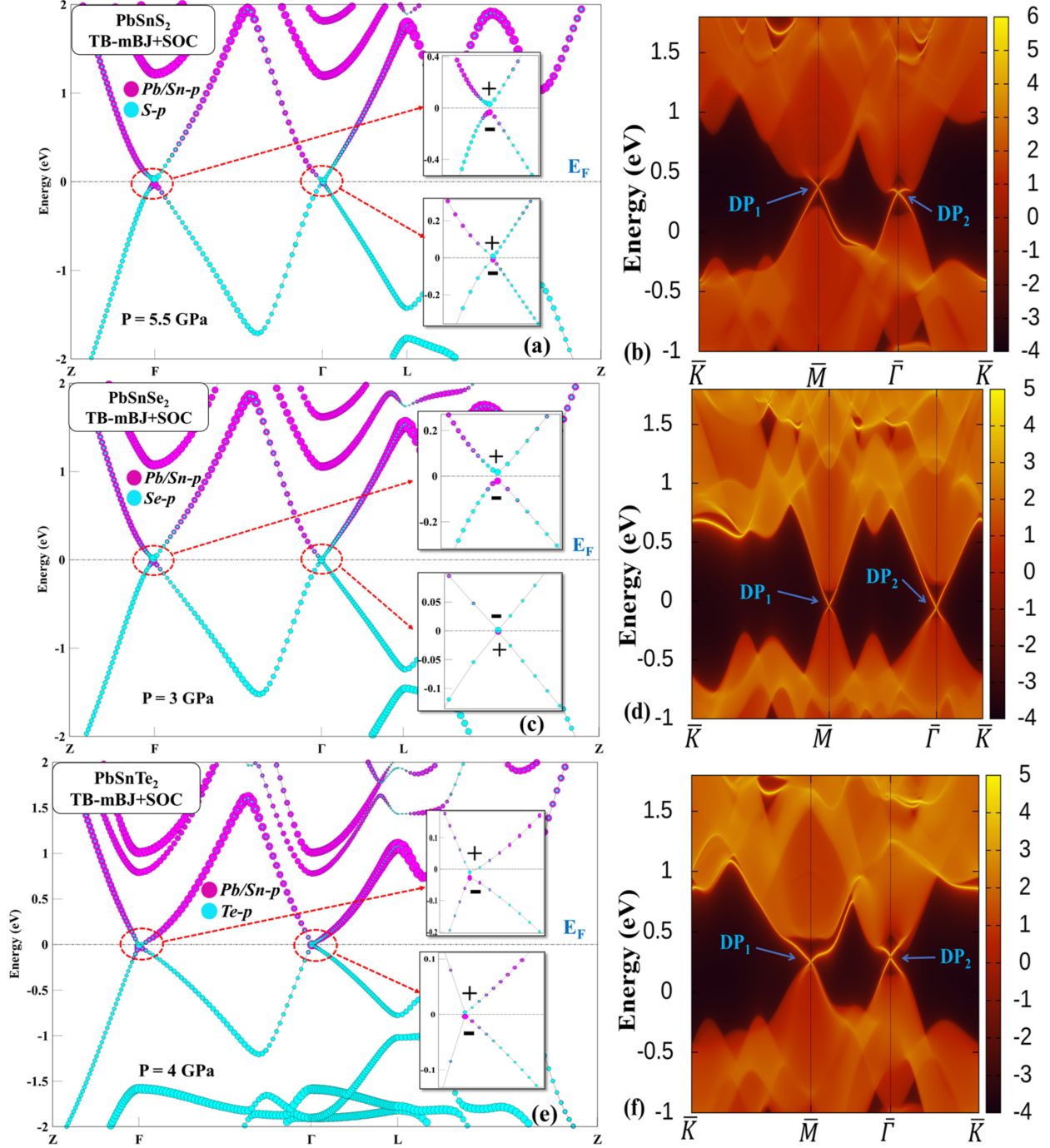


FIG. 4. (a, c, e) The bulk band structure with a pair of band inversions at Γ -point as well as F -point, (b, d, f) The density of states (SODS) along (111) plane of the systems PbSnX_2 (X=S, Se, Te) at elevated pressure with marked Dirac points (DP_1) and (DP_2).

TABLE II. The product of parities of all valance bands at TRIM points and Z_2 invariants under different values of hydrostatic pressure. (The detailed parity tables (TABLE S1-S3) are in supplementary information).

Materials	Hydrostatic Pressure (in GPa)	Γ	$\mathcal{3}L$	$\mathcal{3}F$	Z	Z_2 -invariants
PbSnS ₂	0	+	-	+	-	(0; 000)
	5	+	-	-	-	(1; 000)
	5.5	-	-	-	-	(0; 000)
PbSnSe ₂	0	+	-	+	-	(0; 000)
	2.5	+	-	-	-	(1; 000)
	3	-	-	-	-	(0; 000)
PbSnTe ₂	0	+	-	+	-	(0; 000)
	3.5	+	-	-	-	(1; 000)
	4	-	-	-	-	(0; 000)

$$(-1)^{\nu_0} = \prod_{n_j=0,1} \delta_{n_1 n_2 n_3} \quad (1)$$

$$(-1)^{\nu_{i=1,2,3}} = \prod_{n_i=1; n_{j \neq i}=0,1} \delta_{n_1 n_2 n_3} \quad (2)$$

Here, δ and n_i are representing the parities of all the occupied bands at TRIM points and reciprocal lattice vectors, respectively. The first Z_2 topological invariant (ν_0) is independent of the choice of primitive reciprocal lattice vectors (b_k) but the other three are dependent. But these other three invariants can be recognized with $G_v \equiv \sum_j v_j b_j$ which belongs to 8 element *mod* 2 reciprocal lattices and can be construed as Miller indices of the reciprocal lattice vector. The calculated four Z_2 topological invariants with the help of the product of parities at TRIM points at ambient and elevated hydrostatic pressures of the PbSnX₂ (X=S, Se, Te) family are manifested in TABLE 2.

At the ambient conditions, using equations 1 and 2, the Z_2 topological invariants ($\nu_0; \nu_1 \nu_2 \nu_3$) are (0;000) for the PbSnX₂ (X=S, Se, Te) family which established the trivial semiconductor nature of this family as observed in bulk band structures (FIG. 2 (a, c, e)). When we have applied hydrostatic pressures of 5 GPa, 2.5 GPa and 3.5 GPa on PbSnX₂ (X=S, Se, Te) materials, respectively, the first Z_2 topological invariant (ν_0 switched to 1 (equation 1) and

using equation 2 the other three invariants ($\nu_1\nu_2\nu_3$) remain (000). The non-zero value of (ν_0) recognized these materials as strong TIs at the mentioned pressures. With further increase in pressures to 5.5 GPa, 3 GPa and 4 GPa for the PbSnX_2 ($X=\text{S, Se, Te}$) family, respectively, the value of (ν_0) again switched from 1 to 0 (equation 1) with existence of a pair of band inversions in the bulk band structure. Now, the systems can be topologically weak or trivial in nature depending upon the values of the remaining three invariants ($\nu_1\nu_2\nu_3$) under these pressure conditions. These remaining invariants ($\nu_1\nu_2\nu_3$) are (000) due to the presence of the same negative parities at all eight TRIM points using equation 2. So, these materials are topologically trivial with an even number of inversions under above mentioned elevated hydrostatic pressures.

E. Evolution of TI to TCI phase

The non-zero mirror Chern number (MCN) is used to characterize the TCI phase in materials because mirror symmetry protects those Dirac cones that appear in surface electronic structures. The PbSnX_2 ($X=\text{S, Se, Te}$) family has similar surface states to the TCI materials such as SnTe and PbTe [37, 57, 58], therefore, these materials can also hold TCI phase with an even number of Dirac cones in (111) plane. To confirm the TCI phase in this family, we have analyzed the $(\bar{1}2\bar{1})$ surface, which has mirror symmetry around the $(\bar{1}2\bar{1})$ plane. The perpendicular intersection of $(\bar{1}2\bar{1})$ plane with $(\bar{1}0\bar{1})$ plane is along $\bar{\Gamma} - \bar{X}$ k-path as shown in FIG. 1 (c). Since, PbSnX_2 ($X=\text{S, Se, Te}$) materials have a pair of band inversion (FIG. 5) at Γ - and F -points like SnTe material, we have tried to reproduce the circumstances of SnTe in this family of materials. We anticipate the hybridization of Dirac cones at the crossing which are projected on $(\bar{1}2\bar{1})$ surface. This has been confirmed in FIG. 5 (a, c, e), where the hybridization opens an energy gap along $\bar{X} - \bar{\Gamma}$ path near the Fermi level but along the mirror symmetry path $\bar{\Gamma} - \bar{X}$ Dirac cone holds its crossing. This Dirac cone along the $\bar{\Gamma} - \bar{X}$ is protected by mirror symmetry (not TRS) of $(\bar{1}0\bar{1})$ plane. Along the $\bar{S} - \bar{Y} - \bar{\Gamma}$ path in FIG. 5 (b, d, f), an energy gap is opened after hybridization, because the \bar{Y} -point do not lie on the mirror plane $(\bar{1}0\bar{1})$, which is the projection of two F -points [42] from bulk BZ. Hence, the mirror symmetry-protected Dirac cones exist in the PbSnX_2 ($X=\text{S, Se, Te}$) family, and a TI to TCI phase transition occurs after second inversion under hydrostatic pressure.

This existence of TCI phase is further verified with MCN of the PbSnX_2 ($X=\text{S, Se, Te}$)

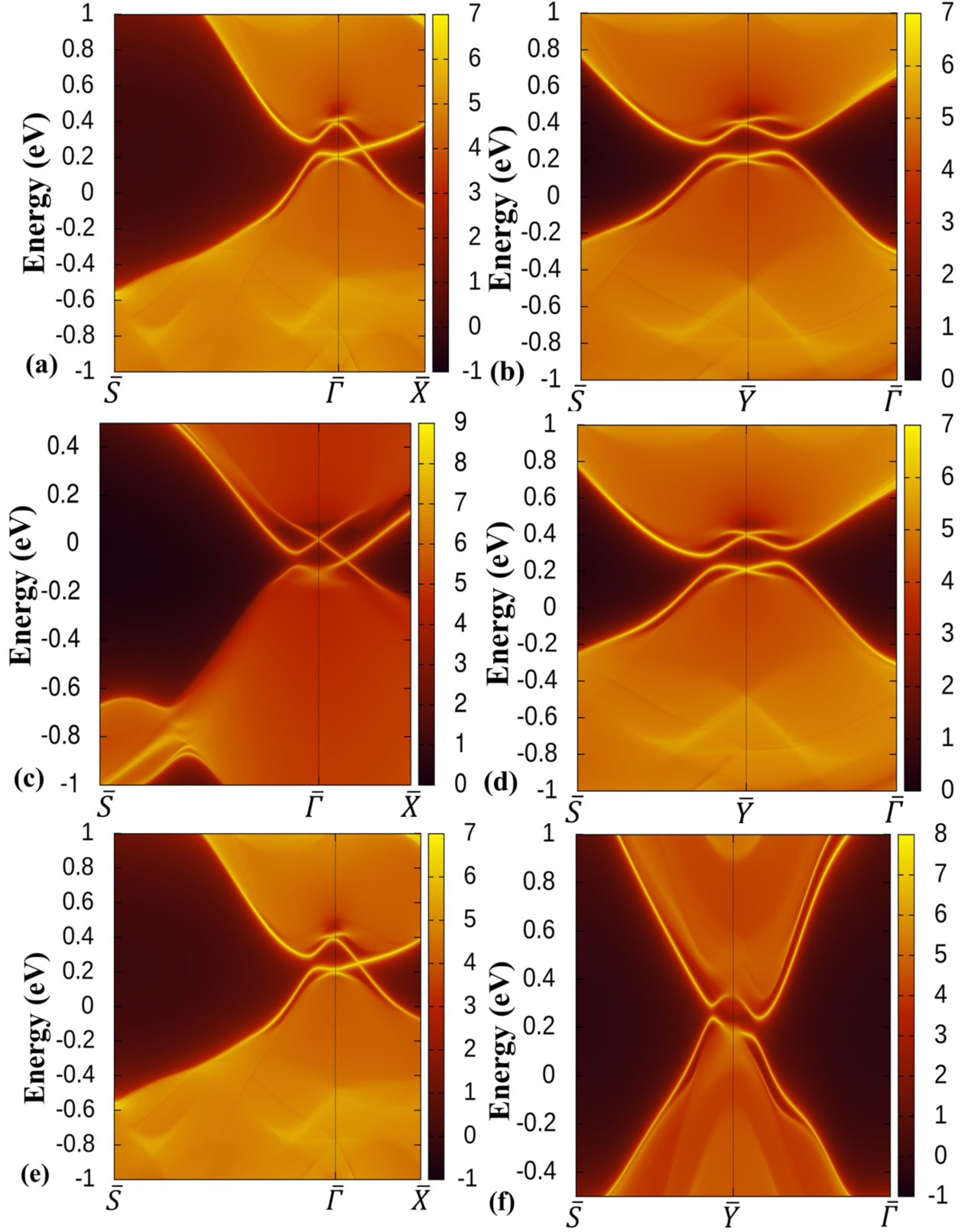


FIG. 5. The SDOS of the slabs (a, b) PbSnS_2 , (c, d) PbSnSe_2 and (e, f) PbSnTe_2 along the $\bar{S} - \bar{\Gamma} - \bar{X}$ and $\bar{S} - \bar{Y} - \bar{\Gamma}$, respectively, with $(\bar{1}2\bar{1})$ oriented planes.

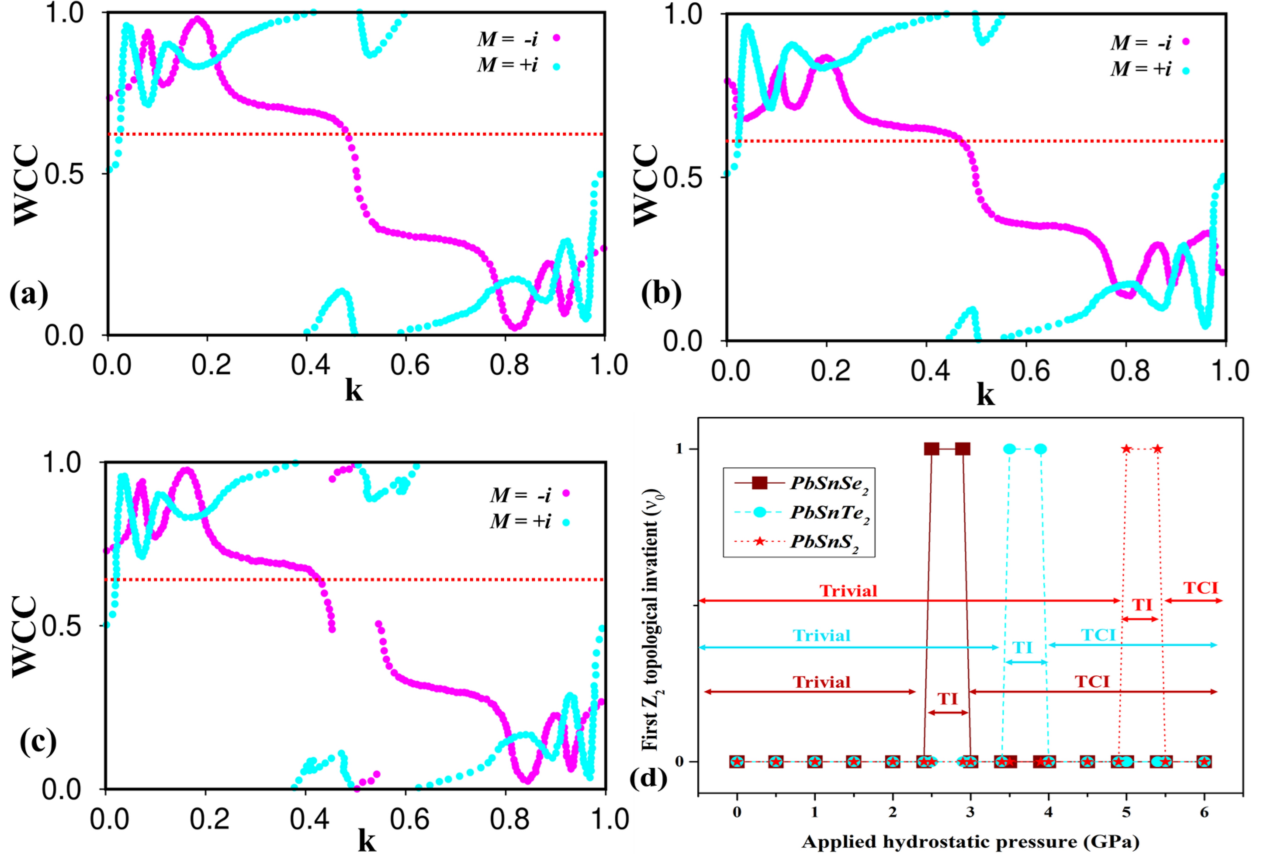


FIG. 6. The evolution of the mirror eigenvalues of $+i$ (magenta) and $-i$ (cyan) in WCC for MCN in (a) $PbSnS_2$, (b) $PbSnSe_2$, and (c) $PbSnTe_2$. (d) The variation of the first Z_2 topological invariant (ν_0) with applied hydrostatic pressure.

materials, with an even number of Dirac cones with respect to the mirror symmetry plane ($\bar{1}0\bar{1}$), which can be calculated using Wannier charge centers (WCC) or Wilson loop along the (111) plane. FIG. 6 (a-c) shows plots of the evolution of WCC for all occupied bands with respect to mirror operator for ($\bar{1}0\bar{1}$) plane. The winding of the WCC of these materials in FIG. 6 (a-c) for mirror eigen values i.e., $+i$ (magenta) and $-i$ (cyan) illustrate that MCN has value 2 along the above-mentioned mirror symmetry. The non-zero even value of MCN and mirror symmetry protected Dirac cone established the TI to TCI phase transitions in $PbSnX_2$ ($X=S, Se, Te$) materials at 5.5 GPa, 3 GPa and 4 GPa, respectively.

The TPT with the variation of the first Z_2 topological invariant (ν_0) with hydrostatic pressure is illustrated in FIG. 6 (d). $PbSnX_2$ ($X=S, Se, Te$) materials have shown a transition from topologically trivial to non-trivial phase with an odd number of inversions under hydrostatic pressure of 5 GPa, 2.5 GPa and 3.5 GPa, respectively. Further increase in pressure has

shown another transition from non-trivial to trivial topological phase and even number of inversions at 5.5 GPa, 3 GPa and 4 GPa, respectively. Moreover, the symmetry analysis with $(\bar{1}0\bar{1})$ mirror plane has shown the TCI phase is achieved after the second transition in these materials with an even number of Dirac cones.

F. CONCLUSION

We have systematically studied the structural stability, and electronic and topological properties of the *Sn-based* ternary chalcogenide PbSnX_2 ($\text{X}=\text{S, Se, Te}$) family under ambient and applied hydrostatic pressure. The TB-mBJ functional has been identified as most relevant *exchange-correlation functionals* for this study based upon the comparative analysis of the band gap of TlBiS_2 , an experimentally synthesized material isostructural to the under-study materials. The phonon dispersion spectrum has confirmed the dynamical stability of these throughout the study. At ambient conditions, TlBiS_2 , PbSnSe_2 and PbSnTe_2 have topologically trivial semiconducting nature with direct band gap of 0.338 eV, 0.183 eV and 0.235 eV at *F-point*. An increase in applied the hydrostatic pressure to 5 GPa, 2.5 GPa and 3.5 GPa, respectively, for PbSnX_2 ($\text{X}=\text{S, Se, Te}$) has led to closing of energy gap at the *F-point*. At these pressure values, the first TPT took place which converts these materials to TIs and the same which has been verified with an odd number of Dirac cones in SDOS and parity analysis at TRIM points. Further enhancement in applied pressure to 5.5 GPa, 3 GPa and 4 GPa, another band inversion has observed at *F-point* in the bulk band structure with an even number of Dirac cones along the (111) plane which make these materials topological trivial again. This topologically trivial phase of these materials, however, has identified as TCI phase along $(\bar{1}2\bar{1})$ surface which holding mirror symmetry for $(\bar{1}0\bar{1})$ plane. The SDOS along the k path $\bar{S}-\bar{\Gamma}-\bar{X}$ and $\bar{S}-\bar{Y}-\bar{\Gamma}$ of $(\bar{1}2\bar{1})$ plane has established the mirror symmetry protection for the Dirac cones. This TCI phase has further corroborated with even value of mirror Chern number calculated using the evolution of mirror eigenvalues $\pm i$ in WCC. This kind of transition from trivial to TI to TCI can also be observed in other similar ternary chalcogenides and the pressure-induced surface states can be further studied experimentally with the help of angle and spin-resolved photoemission spectroscopy.

ACKNOWLEDGMENTS

All the authors acknowledge National Supercomputing Mission (NSM) for providing computing resources of ‘PARAM Siddhi-AI’, under National PARAM Supercomputing Facility (NPSF), C-DAC, Pune and supported by the Ministry of Electronics and Information Technology (MeitY) and Department of Science and Technology (DST), Government of India. One of the authors (Ramesh Kumar) would like to thank the Council of Scientific and Industrial Research (CSIR), Delhi, for financial support.

Author contributions: These authors contributed equally to this work.

Conflict of interest statements: The authors declare no competing financial interest.

References

- [1] M. Z. Hasan, and C. L. Kane, Colloquium: Topological insulators, *Rev. Mod. Phys.* **82**, 3045 (2007).
- [2] X.-L. Qi, and S.-C. Zhang, Topological insulators and superconductors, *Rev. Mod. Phys.* **83**, 1057 (2011).
- [3] H. Zhang, C.-X. Liu, X.-L. Qi, X. Dai, Z. Fang, and S.-C. Zhang, Topological insulators in Bi_2Se_3 , Bi_2Te_3 and Sb_2Te_3 with a single dirac cone on the surface, *Nat. Phys.* **5**, 438 (2009).
- [4] Y. L. Chen, J. G. Analytis, J.-H. Chu, Z. K. Liu, S.-K. Mo, X. L. Qi, H. J. Zhang, D. H. Lu, X. Dai, Z. Fang, S. C. Zhang, I. R. Fisher, Z. Hussain, and Z.-X. Shen, Experimental realization of a three-dimensional topological insulator, Bi_2Te_3 , *Science* **325**, 178 (2009).
- [5] Y. Xia, D. Qian, D. Hsieh, L. Wray, A. Pal, H. Lin, A. Bansil, D. Grauer, Y. S. Hor, R. J. Cava, and M. Z. Hasan, Observation of a large-gap topological-insulator class with a single dirac cone on the surface, *Nat. Phys.* **5**, 398 (2009).
- [6] L. Fu and C. L. Kane, Topological insulators with inversion symmetry, *Phys. Rev. B* **76**, 045302 (2007).
- [7] L. Fu, Topological crystalline insulators, *Phys. Rev. Lett.* **106**, 106802 (2011).
- [8] T. H. Hsieh, H. Lin, J. Liu, W. Duan, A. Bansil, and L. Fu, Topological crystalline insulators in the SnTe material class, *Nat. Commun.* **3**, 982 (2012).

- [9] Y. Tanaka, Z. Ren, T. Sato, K. Nakayama, S. Souma, T. Takahashi, K. Segawa, and Y. Ando, Experimental realization of a topological crystalline insulator in SnTe, *Nat. Phys.* **8**, 800 (2012).
- [10] Z. Wang, Y. Sun, X.-Q. Chen, C. Franchini, G. Xu, H. Weng, X. Dai, and Z. Fang, Dirac semimetal and topological phase transitions in A_3Bi ($A = Na, K, Rb$), *Phys. Rev. B* **85**, 195320 (2012).
- [11] Z. K. Liu, B. Zhou, Y. Zhang, Z. J. Wang, H. M. Weng, D. Prabhakaran, S.-K. Mo, Z. X. Shen, Z. Fang, X. Dai, Z. Hussain, and Y. L. Chen, Discovery of a three-dimensional topological dirac semimetal, NaBi, *Science* **343**, 864 (2014).
- [12] B. Q. Lv, H. M. Weng, B. B. Fu, X. P. Wang, H. Miao, J. Ma, P. Richard, X. C. Huang, L. X. Zhao, G. F. Chen, Z. Fang, X. Dai, T. Qian, and H. Ding, Experimental discovery of Weyl semimetal TaAs, *Phys. Rev. X* **5**, 031013 (2015).
- [13] S.-Y. Xu, I. Belopolski, N. Alidoust, M. Neupane, G. Bian, C. Zhang, R. Sankar, G. Chang, Z. Yuan, C.-C. Lee, S.-M. Huang, H. Zheng, J. Ma, D. S. Sanchez, B. Wang, A. Bansil, F. Chou, P. P. Shibayev, H. Lin, S. Jia, and M. Z. Hasan, Discovery of a Weyl fermion semimetal and topological Fermi arcs, *Science* **349**, 613 (2015).
- [14] Q. Xu, Z. Song, S. Nie, H. Weng, Z. Fang, and X. Dai, Two-dimensional oxide topological insulator with iron-pnictide superconductor LiFeAs structure, *Phys. Rev. B* **92**, 205310 (2015).
- [15] J. Hu, Z. Tang, J. Liu, X. Liu, Y. Zhu, D. Graf, K. Myhro, S. Tran, C. N. Lau, J. Wei, and Z. Mao, Evidence of topological nodal-line fermions in ZrSiSe and ZrSiTe, *Phys. Rev. Lett.* **117**, 016602 (2016).
- [16] S. Khalid, F. P. Sabino, and A. Janotti, Topological phase transition in LaAs under pressure, *Phys. Rev. B* **98**, 220102 (2018).
- [17] P.-J. Guo, H.-C. Yang, K. Liu, and Z.-Y. Lu, Theoretical study of the pressure-induced topological phase transition in LaSb, *Phys. Rev. B* **96**, 081112 (2017).
- [18] J.-Z. Ma, J.-B. He, Y.-F. Xu, B. Q. Lv, D. Chen, W.-L. Zhu, S. Zhang, L.-Y. Kong, X. Gao, L.-Y. Rong, Y.-B. Huang, P. Richard, C.-Y. Xi, E. S. Choi, Y. Shao, Y.-L. Wang, H.-J. Gao, X. Dai, C. Fang, H.-M. Weng, G.-F. Chen, T. Qian, and H. Ding, Three-component fermions with surface fermi arcs in tungsten carbide, *Nat. Phys.* **14**, 349 (2018).
- [19] J. B. He, D. Chen, W. L. Zhu, S. Zhang, L. X. Zhao, Z. A. Ren, and G. F. Chen, Magnetotransport properties of the triply degenerate node topological semimetal tungsten carbide,

- Phys.Rev. B* **95**, 195165 (2017).
- [20] J. E. Moore, The birth of topological insulators, *Nature* **464**, 194 (2010).
- [21] M. He, H. Sun, and Q. L. He, Topological insulator: Spintronics and quantum computations, *Front. Phys.* **14**, 43401 (2019).
- [22] Y. Fan and K. L. Wang, Spintronics based on topological insulators, *SPIN* **06**, 1640001 (2016).
- [23] X. Li, D. Chen, M. Jin, D. Ma, Y. Ge, J. Sun, W. Guo, H. Sun, J. Han, W. Xiao, J. Duan, Q. Wang, C.-C. Liu, R. Zou, J. Cheng, C. Jin, J. Zhou, J. B. Goodenough, J. Zhu, and Y. Yao, Pressure-induced phase transitions and superconductivity in a quasi 1-dimensional topological crystalline insulator α -Bi₄Br₄, *Proceedings of the National Academy of Sciences* **116**, 17696 (2019).
- [24] M. Singh, R. Kumar, and R. K. Bibiyan, Pressure-induced topological phase transition in XMR material YbAs: a first-principles study, *Eur. Phys. J. Plus* **137**, 633 (2022).
- [25] P. Wadhwa, S. Kumar, A. Shukla, and R. Kumar, First principles investigation of topological phase in XMR material TmSb under hydrostatic pressure, *J Phys Condens Matter.* **31**, 335401 (2019).
- [26] P. Wadhwa, S. Kumar, A. Shukla, and R. Kumar, Studies of non-trivial band topology and electron-hole compensation in YSb, *Solid State Commun.* **321**, 114022 (2020).
- [27] R. Kumar and M. Singh, Topological phase transition and tunable surface states in YBi, *J. Phys. Condens. Matter* **36**, 345601 (2020).
- [28] I. Y. Sklyadneva, I. P. Rusinov, R. Heid, K.-P. Bohnen, P. M. Echenique, and E. V. Chulkov, Pressure-induced topological phases of KNa₂Bi, *Sci. Rep.* **6**, 24137 (2016).
- [29] Y. Qi, W. Shi, P. G. Naumov, N. Kumar, R. Sankar, W. Schnelle, C. Shekhar, F.-C. Chou, C. Felser, B. Yan, and S. A. Medvedev, Topological quantum phase transition and superconductivity induced by pressure in the bismuth tellurohalide BiTeI, *Adv. Mater.* **29**, 1605965 (2017).
- [30] M. Yang, Y. Z. Luo, M. G. Zeng, L. Shen, Y. H. Lu, J. Zhou, S. J. Wang, I. K. Sou, and Y. P. Feng, Pressure induced topological phase transition in layered Bi₂S₃, *Phys. Chem. Chem. Phys.* **19**, 29372 (2017).
- [31] A. Ohmura, Y. Higuchi, T. Ochiai, M. Kanou, F. Ishikawa, S. Nakano, A. Nakayama, Y. Yamada, and T. Sasagawa, Pressure-induced topological phase transition in the polar semiconductor BiTeBr, *Phys. Rev. B* **95**, 125203 (2017).

- [32] H. Ozawa, A. Yamakage, M. Sato, and Y. Tanaka, Topological phase transition in a topological crystalline insulator induced by finite-size effects, *Phys. Rev. B* **90**, 045309 (2014).
- [33] M. Ezawa, Topological switch between second-order topological insulators and topological crystalline insulators, *Phys. Rev. Lett.* **121**, 116810 (2018).
- [34] W. A. Benalcazar, T. Li, and T. L. Hughes, Quantization of fractional corner charge in Cnsymmetric higher-order topological crystalline insulators, *Phys. Rev. B* **99**, 245151 (2019).
- [35] S.-Y. Xu, C. Liu, N. Alidoust, M. Neupane, D. Qian, I. Belopolski, J. D. Denlinger, Y. J. Wang, H. Lin, L. A. Wray, G. Landolt, B. Slomski, J. H. Dil, A. Marcinkova, E. Morosan, Q. Gibson, R. Sankar, F. C. Chou, R. J. Cava, A. Bansil, and M. Z. Hasan, Observation of a topological crystalline insulator phase and topological phase transition in $\text{Pb}_{1-x}\text{Sn}_x\text{Te}$, *Nat. Commun.* **3**, 1192 (2012).
- [36] P. Dziawa, B. J. Kowalski, K. Dybko, R. Buczko, A. Szczerbakow, M. Szot, E. Lusakowska, T. Balasubramanian, B. M. Wojek, M. H. Berntsen, O. Tjernberg, and T. Story, Topological crystalline insulator states in $\text{Pb}_{1-x}\text{Sn}_x\text{Se}$, *Nat. Mater.* **11**, 1023 (2012).
- [37] S. Ma, C. Guo, C. Xiao, F. Wu, M. Smidman, Y. Lu, H. Yuan, and H. Wu, Realization of a new topological crystalline insulator and lifshitz transition in PbTe , *Adv. Funct. Mater.* **28**, 1803188 (2018).
- [38] Y. Sun, Z. Zhong, T. Shirakawa, C. Franchini, D. Li, Y. Li, S. Yunoki, and X.-Q. Chen, Rocksalt SnS and SnSe : Native topological crystalline insulators, *Phys. Rev. B* **88**, 235122 (2013).
- [39] C. Niu, P. M. Buhl, G. Bihlmayer, D. Wortmann, S. Blügel, and Y. Mokrousov, Twodimensional topological crystalline insulator and topological phase transition in TlSe and TlS monolayers, *Nano Lett.* **15**, 6071 (2015).
- [40] H. Lin, R. S. Markiewicz, L. A. Wray, L. Fu, M. Z. Hasan, and A. Bansil, Single-dirac-cone topological surface states in the TlBiSe_2 class of topological semiconductors, *Phys. Rev. Lett.* **105**, 036404 (2010).
- [41] S. V. Eremeev, G. Bihlmayer, M. Vergniory, Y. M. Koroteev, T. V. Menshchikova, J. Henk, A. Ernst, and E. V. Chulkov, Ab initio electronic structure of thallium-based topological insulators, *Phys. Rev. B* **83**, 205129 (2011).
- [42] Q. Zhang, Y. Cheng, and U. Schwingenschlögl, Emergence of topological and topological crystalline phases in TlBiS_2 and TlSbS_2 , *Sci. Rep.* **5**, 8379 (2015).

- [43] P. Hohenberg and W. Kohn, Inhomogeneous electron gas, *Phys. Rev.* **136**, B864 (1964).
- [44] W. Kohn and L. J. Sham, Self-consistent equations including exchange and correlation effects, *Phys. Rev.* **140**, A1133 (1965).
- [45] G. Kresse and D. Joubert, From ultrasoft pseudopotentials to the projector augmented-wave method, *Phys. Rev. B* **59**, 1758 (1999).
- [46] G. Kresse and J. Furthmüller, Efficient iterative schemes for ab initio total-energy calculations using a plane-wave basis set, *Phys. Rev. B* **54**, 11169 (1996).
- [47] J. P. Perdew, K. Burke, and M. Ernzerhof, Generalized gradient approximation made simple, *Phys. Rev. Lett.* **77**, 3865 (1996).
- [48] F. Tran and P. Blaha, Accurate band gaps of semiconductors and insulators with a semilocal exchange-correlation potential, *Phys. Rev. Lett.* **102**, 226401 (2009).
- [49] A. Togo and I. Tanaka, First principles phonon calculations in materials science, *Scr. Mater.* **108**, 1 (2015).
- [50] N. Marzari, A. A. Mostofi, J. R. Yates, I. Souza, and D. Vanderbilt, Maximally localized wannier functions: Theory and applications, *Rev. Mod. Phys.* **84**, 1419 (2012).
- [51] Q. Wu, S. Zhang, H.-F. Song, M. Troyer, and A. A. Soluyanov, Wanniertools: An open-source software package for novel topological materials, *Comput. Phys. Commun.* **224**, 405 (2018).
- [52] M. Ozer, K. M. Paraskevopoulos, A. N. Anagnostopoulos, S. Kokou, and E. K. Polychroniadis, Large single-crystal growth and characterization of the narrow-gap semiconductor, *Semicond. Sci. Technol.* **11**, 1405 (1996).
- [53] B. Singh, H. Lin, R. Prasad, and A. Bansil, Topological phase transition and quantum spin Hall state in TlBiS₂, *J. Appl. Phys.* **116**, 033704 (2014).
- [54] A. N. Veis, D. D. Koditsa, and N. S. Popovich, Optical properties of TlBiS₂ monocrystals, *physica status solidi (a)* **107**, K169 (1988).
- [55] O. Valassiades, E. K. Polychroniadis, J. Stoemenos, and N. A. Economou, On the disordered nature of single crystalline TlBiTe₂ and its influence on its electrical properties, *physica status solidi (a)* **65**, 215 (1981).
- [56] C. L. Mitsas, D. I. Siapkias, E. K. Polychroniadis, O. Valassiades, and K. M. Paraskevopoulos, Growth, electrical, and optical properties of TlBiSe₂ single crystals, *physica status solidi (a)* **136**, 483 (1993).
- [57] Y. Tanaka, Z. Ren, T. Sato, K. Nakayama, S. Souma, T. Takahashi, K. Segawa, and Y.

Ando, Experimental realization of a topological crystalline insulator in SnTe, *Nat. Phys.* **8**, 800 (2012).

- [58] T. H. Hsieh, H. Lin, J. Liu, W. Duan, A. Bansil, and L. Fu, Topological crystalline insulators in the SnTe material class, *Nat. Commun.* **3**, 982 (2012).